INSTITUTE OF PHYSICS PUBLISHING JOURNAL OF PHYSICS B: ATOMIC, MOLECULAR AND OPTICAL PHYSICS

J. Phys. B: At. Mol. Opt. Phys. **36** (2003) 2629–2645 PII: S0953-4075(03)60054-4

Electron-impact emission cross-sections for the 5p → 5s and 5s → 4p transitions of Kr I

S Tsurubuchi, H Kobayashi and M Hyodo

Department of Applied Physics, Faculty of Technology, Tokyo University of Agriculture and Technology, Naka-cho 2-24-16, Koganei-shi, Tokyo 184-8588, Japan

Received 21 February 2003, in final form 6 May 2003
Published 10 June 2003
Online at stacks.iop.org/JPhysB/36/2629

Abstract

Electron-impact emission cross-sections of Kr were measured from the threshold to 1000 eV for the 5p → 5s transition in visible to near infrared regions and for the 5s → 4p resonance lines (116.49 and 123.58 nm) in the VUV region. The experiment was carried out at sufficiently low target pressure to ensure a single collision between an electron and an atom since previously published works show rather large scattering not only in the magnitude, but also in the energy dependence of emission cross-sections, probably because of high target pressures. Absolute emission cross-sections for resonance lines were obtained by normalizing relative cross-sections at effectively zero target pressure to that of hydrogen Lyman-α produced in electron impact of H_2. Level excitation cross-sections of the $1s_2$ and $1s_4$ states (Paschen notation) were obtained by subtracting the total cascade 5p → 5s cross-sections from corresponding emission cross-sections of the 116.49 and 123.58 nm resonance lines. Obtained results are compared with other experimental and theoretical data.

1. Introduction

The emission cross-section of rare gases is important for many fields including discharge physics, plasma physics, astrophysics, laser physics and so on. Emission cross-sections for the np → ns transition and ns → $(n-1)$p resonant transition of neutral species (Ne, $n = 3$; Ar, $n = 4$) have been studied systematically in previous works (Tsurubuchi *et al* 1996, 2000) as well as the 4p → 4s laser transition of Ar^+ (Tsurubuchi 1997).

For the 5p → 5s transitions of Kr, experimental emission cross-sections were given by Feltsan (1967) below 100 eV, Bogdanova and Yurgenson (1987) for two high energies (100 and 200 eV) and peak cross-section values, Gay *et al* (1996) for the $2p_9$ → $1s_5$ transition below 100 eV and Chilton *et al* (2000) up to 200 eV by optical detection of emitted radiation. There remains, however, dissonance among experimental results, requiring further accumulation and

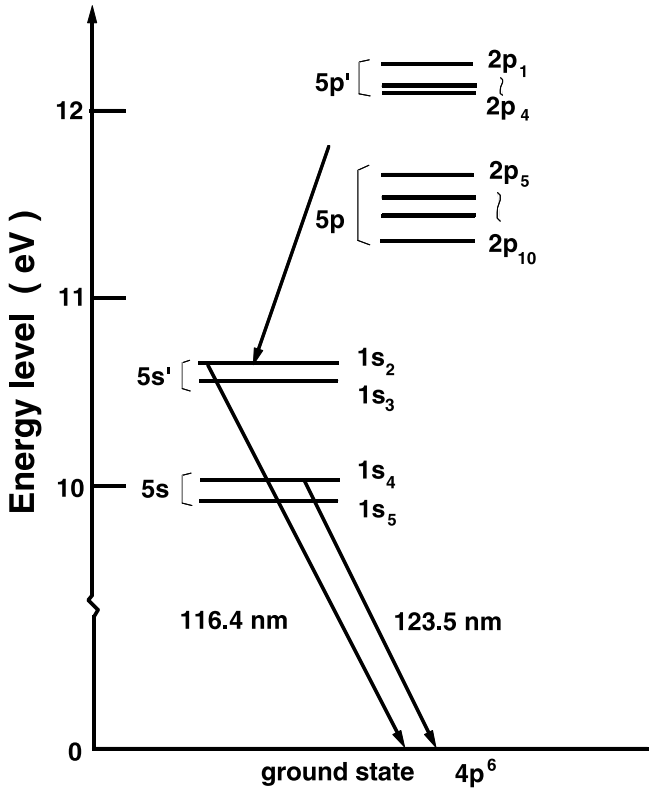

Figure 1. Energy-level diagram of the low lying excited levels of Kr I in the Paschen notation. The ion-core state of the unprimed levels is $4p^5\ ^2P_{3/2}$ whereas it is $4p^5\ ^2P_{1/2}$ for the primed levels.

appraisal of data. Figure 1 shows an energy-level diagram of Kr with related spectroscopic notations.

Theoretically, Kaur *et al* (1998) presented a relativistic distorted-wave (RDWA) calculation for the 5p → 5s transitions. Dasgupta *et al* (2001) reported systematic theoretical works for the $4p^5 5s$ and $4p^5 5p$ levels by distorted-wave (DW-1, DW-2) and semirelativistic Breit–Pauli *R*-matrix (BPRM) approaches with a varying number of states (5, 15 or 51) included in close-coupling expansion.

There have been no experimental reports addressing emission cross-sections of the 5s → 4p resonance lines (116.49 and 123.58 nm) of Kr. Level excitation cross-sections for the $1s_2(5s'[1/2]^o_1)$ and $1s_4(5s[3/2]^o_1)$ states were given by Trajmar *et al* (1981), Takayanagi *et al* (1990) and Guo *et al* (2000) by energy loss measurements. A set of theoretical excitation cross-sections was presented by Dasgupta *et al* (2001).

2. Experimental details

The experimental apparatus is essentially the same as that presented in previous works for Ne and Ar (Tsurubuchi *et al* 1996, 2000, Tsurubuchi 1997), except for a newly made collision chamber with 30 cm outer diameter. Briefly, the system was pumped out by a turbo-molecular pump. A 50 cm visible monochromator and a Seya–Namioka vacuum monochromator were used for spectral line-intensity measurements. The diameter of the Rowland circle of the

VUV monochromator was 498.1 mm. A Cu–BeO plate coated with caesium iodide served as a photo-cathode to enhance the detection efficiency of a channel electron multiplier. The electron beam was modulated for synchronous single-photon-counting measurement.

Krypton gas was introduced continuously through a needle valve to fill the collision chamber uniformly. Interior pressure was kept constant during measurement and monitored by a Bayard–Alpert ionization gauge for which sensitivity for different kind of gas was calibrated with a capacitance manometer (MKS Baratron; MKS Inc.). When ionization gauge output was plotted against that of the capacitance manometer, a straight line drawn by the method of least squares through the data points came very close to the point of zero pressure. The proportionality constant depends on the kind of gas. Output linearity of the ionization gauge was fairly good over the pressure range calibrated. Gas temperature in the chamber must be known to convert the value of pressure into number density of ground-state atoms. During measurement, the wall temperature of the collision chamber was carefully monitored: the temperature change was very small during measurement, probably because of the large heat capacity of the chamber.

The optical sensitivity of the detection system $k(\lambda)$ at wavelength λ in the visible range was measured with a calibrated standard lamp in the wavelength range of 400–750 nm. Above 750 nm, sensitivity was determined by measuring several line pairs of Ar with known branching ratios (Wiese *et al* 1969, 1989). The absolute cross-section for the 5p → 5s transitions was obtained by comparing line intensities with that of the Ar 750.3 nm line, for which an emission cross-section was obtained by absolute measurement of line intensity (Tsurubuchi *et al* 1996). Well established emission cross-sections of He lines presented by van Zyl *et al* (1980) were used to confirm obtained results.

An absolute sensitivity of the detection system in the VUV region was obtained by comparing measured intensities of band spectra of H_2 with those calibrated ones presented by Ajello *et al* (1988) (Tsurubuchi *et al* 1991, 1994). The overlapped component must be subtracted from the line intensity, because the Lyman-α line of the H atom produced from the H_2 molecule is superposed by molecular bands (Shemansky *et al* 1985). Relative emission cross-sections for resonance lines at effectively zero pressure were normalized to a mean absolute emission cross-section, 7.3×10^{-18} cm^2, at 100 eV of the hydrogen Lyman-α line produced in electron impact of H_2 (Ligtenberg *et al* 1985, Woolsey *et al* 1986, Shemansky *et al* 1985, van Zyl *et al* 1985, Ajello *et al* 1988). Because of strong self-absorption, relative emission cross-sections for the $5s'[1/2]^o_1 \rightarrow 4p\ ^1S_0$ (116.49 nm line) and $5s[3/2]^o_1 \rightarrow 4p\ ^1S_0$ (123.58 nm lines) transitions at effectively zero pressure $(S/IP)_{P\rightarrow 0}$ were obtained by extrapolation of data points, where S is the signal output and I and P are incident current and target pressure, respectively. Experimentally obtained transmission curves, $T_R = \frac{(S/IP)}{(S/IP)_{P\rightarrow 0}}$, were compared with calculated ones obtained by use of established values of optical oscillator strengths for these transitions. Target pressure was kept as low as 7.3×10^{-4} Pa during measurements of relative excitation function, to reduce the possible effect of radiation trapping.

Measurements were all carried out under the condition of a single collision between an electron and a target atom, i.e. under the condition that the output signal is always proportional to target pressure and to electron-beam current. Figure 2 shows the pressure dependence of the 758.7 nm line ($2p_5 \rightarrow 1s_4$) at 25 and 85 eV. Linearity holds in a wide range of target pressure at 25 eV, while it is quadratic at 85 eV. The emission intensity for the $2p_9 \rightarrow 1s_5$ line shows slight downward deviation from a straight line above about 2.7×10^{-2} Pa, as shown in figure 3. The effect of self-absorption may play a role because the $1s_5$ level is a metastable state. Therefore, present measurements for the 5p → 5s group were all performed at target pressure below 6.7×10^{-3} Pa, which was kept constant during measurement. The distance between the centre of the chamber and an observation window is 25.3 cm in the present setting.

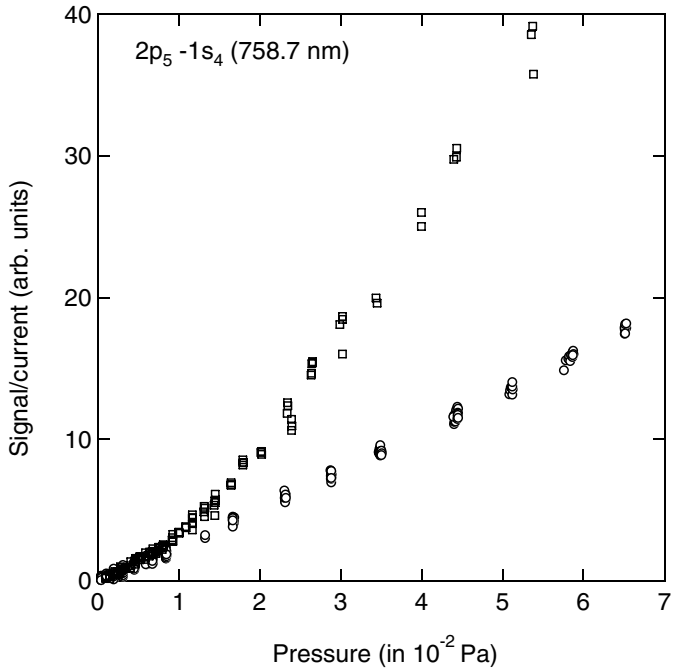

Figure 2. Pressure dependence of emission intensity of 758.7 nm line ($2p_5 \rightarrow 1s_4$): O at 25 eV and □ at 85 eV.

Although the output signal had a linear current dependence up to about 2 mA, the electron current was usually kept below 1 mA.

The total radiation intensity of the $j \rightarrow k$ transition, per unit time, per unit length of the electron beam, is given by $J_{jk} = NQ_{jk}i/e$, where N is gas density, i and e are the current and charge of the incident electron beam, respectively, and Q_{jk} is the effective cross-section or emission cross-section of the $j \rightarrow k$ transition. In equilibrium, J_{jk} is given as

$$J_{jk} = \frac{A_{jk}}{A_j}\left(NQ_j\frac{i}{e} + \sum_{i>j} J_{ij}\right), \tag{1}$$

where A_{jk} is the probability/s of the radiative transition from the jth to the kth level, Q_j is the cross-section for excitation of the jth level (Massey and Burhop 1969) and

$$A_j = \sum_{k<j} A_{jk} \qquad \text{and} \qquad A_{jk}/A_j = J_{jk}\Big/\sum_{k<j} J_{jk}. \tag{2}$$

Taking summation over k, we have, in terms of (1),

$$\sum_{k<j} Q_{jk} = Q_j + \sum_{i>j} Q_{ij} \equiv Q_j^{apparent}. \tag{3}$$

The second term, $\sum_{i>j} Q_{ij}$, represents the summed cascade cross-section to the jth level; $\sum_{k<j} Q_{jk}$ is the sum of emission cross-sections from the jth level. $Q_j^{apparent}$ is the apparent excitation cross-section of the jth level including cascade transitions.

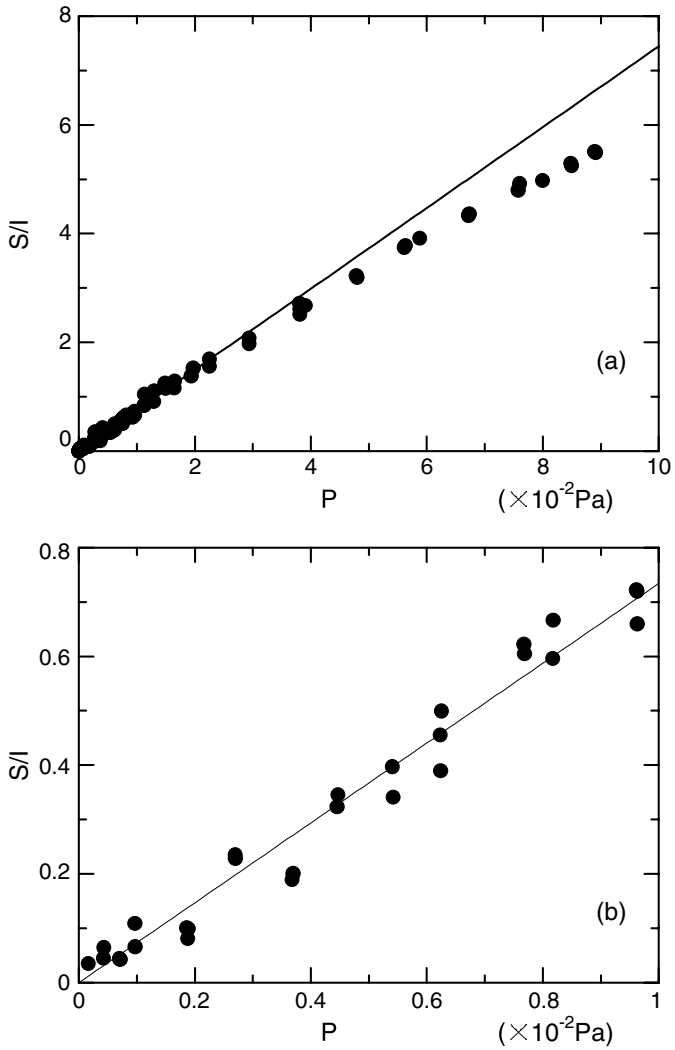

Figure 3. Pressure dependence of emission intensities: ●, 811.29 nm ($2p_9 \rightarrow 1s_5$) line at 100 eV.

3. Results and discussion

3.1. Emission cross-sections for the 5p → 5s transition

Figures 4–7 show 'apparent excitation cross-sections', $Q_{2p_i}^{apparent}$, for $2p_i$ ($i = 1$–10) states. Table 1 presents emission cross-sections for each spectral line. For those spectral lines with moderate intensity, the absolute value of emission cross-section was measured. Other numerical values in the same line of the table were determined using branching ratios of Dzierżęga *et al* (2000), because energy dependence should be identical among those transitions with a common upper state. $Q_{2p_i}^{apparent}$ is obtained by summing up those values in the same line. Therefore, each emission cross-section in the same line can be obtained, in turn, by multiplying $Q_{2p_i}^{apparent}$ by the ratio of spontaneous transition probabilities of related transitions.

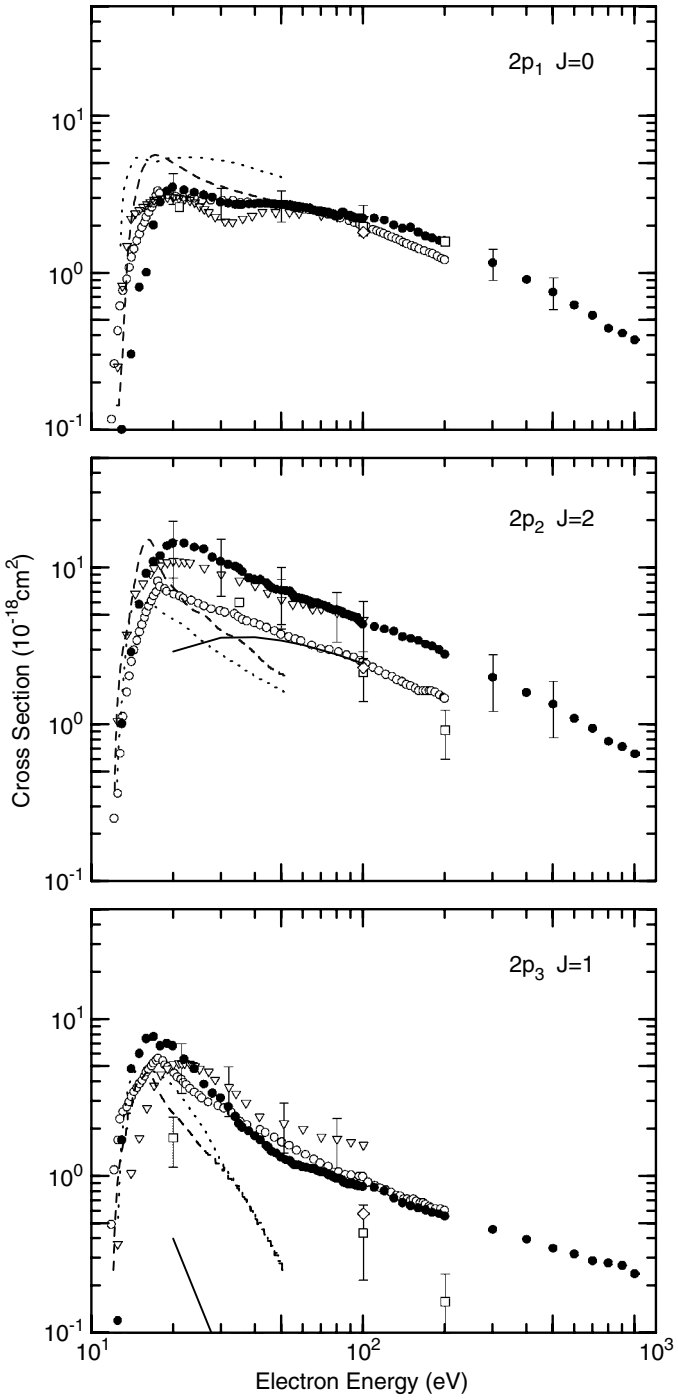

Figure 4. Cross-sections for $2p_1$–$2p_3$. Apparent cross-sections (see equation (3)): ●, present work; ○, Chilton *et al* (2000) at 2.7×10^{-1}Pa; ▽, Feltsan (1967); excitation cross-section: □, Bogdanova and Yurgenson (1987); ◇, Chilton *et al* (2000) at 1.3×10^{-2}Pa; the dotted curves represent the distorted wave calculation DW-1 (Dasgupta *et al* 2001); long-dashed curves, 15-state BPRM results (Dasgupta *et al* 2001); full curves, distorted wave calculation MCGS (Kaur *et al* 1998). The 15-state BPRM for $2p_1$ is $\times 0.1$.

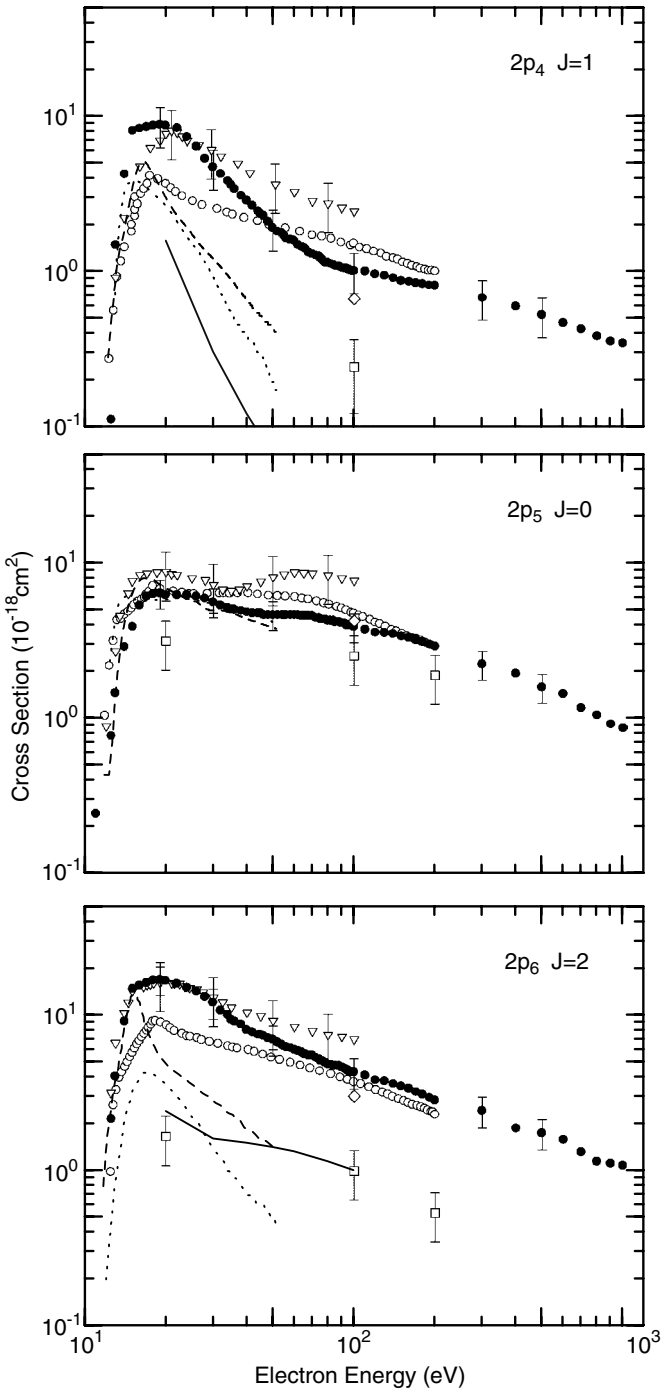

Figure 5. Cross-sections for $2p_4$–$2p_6$. Apparent cross-sections: ●, present work; ○, Chilton *et al* (2000) at 2.7×10^{-1} Pa; ▽, Feltsan (1967); excitation cross-section: □, Bogdanova and Yurgenson (1987); ◇, Chilton *et al* (2000) at 1.3×10^{-2} Pa; the dotted curves represent the distorted wave calculation DW-1 (Dasgupta *et al* 2001); long-dashed curves, 15-state BPRM results (Dasgupta *et al* 2001); full curves, distorted wave calculation MCGS (Kaur *et al* 1998). The 15-state BPRM for $2p_5$ states is ×0.2.

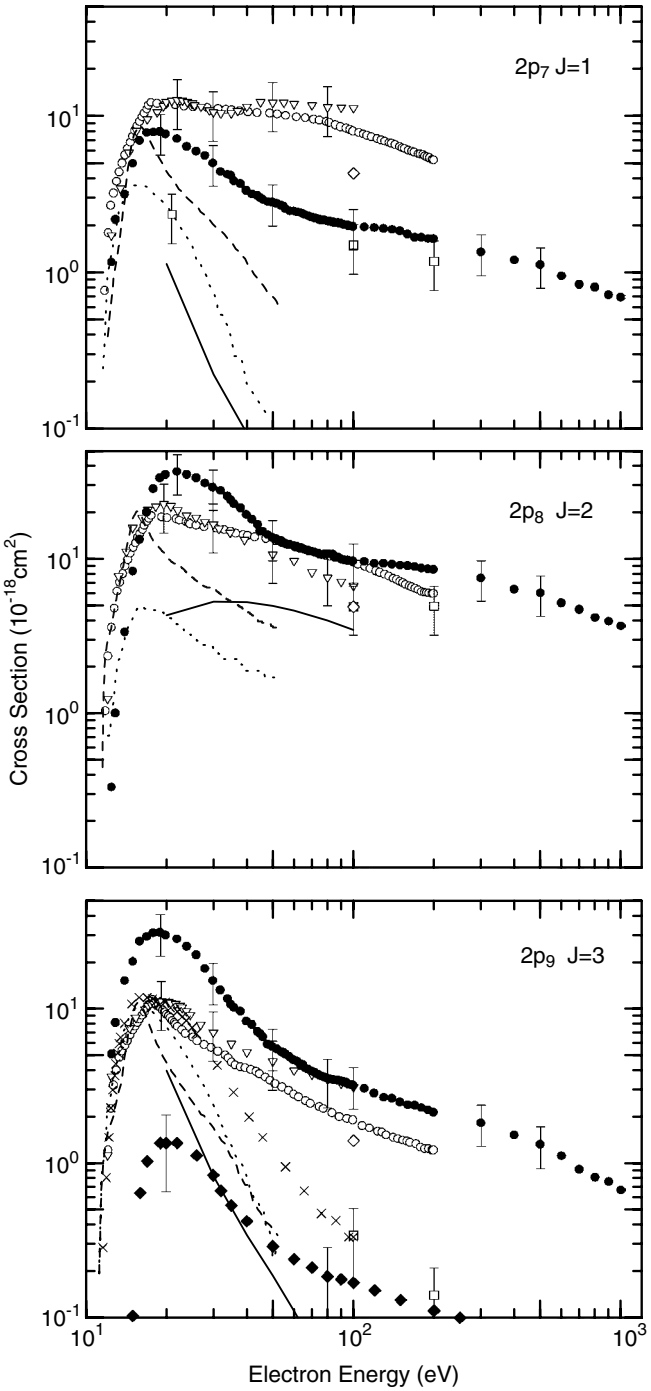

Figure 6. Cross-sections for $2p_7$–$2p_9$. Apparent cross-sections: ●, present work; ○, Chilton *et al* (2000) at 2.7×10^{-1} Pa; ▽, Feltsan (1967); excitation cross-section: □, Bogdanova and Yurgenson (1987); ◇, Chilton *et al* (2000) at 1.3×10^{-2} Pa; ×, Gay *et al* (1996); ◆, one cascade emission cross-section for the $2p_9$ state (645.6 nm curve, $6d[7/2]_4 \rightarrow 5p[5/2]_3$); the dotted curves represent the distorted wave calculation DW-1 (Dasgupta *et al* 2001); long-dashed curves, 15-state BPRM results (Dasgupta *et al* 2001); full curves, distorted wave calculation MCGS (Kaur *et al* 1998).

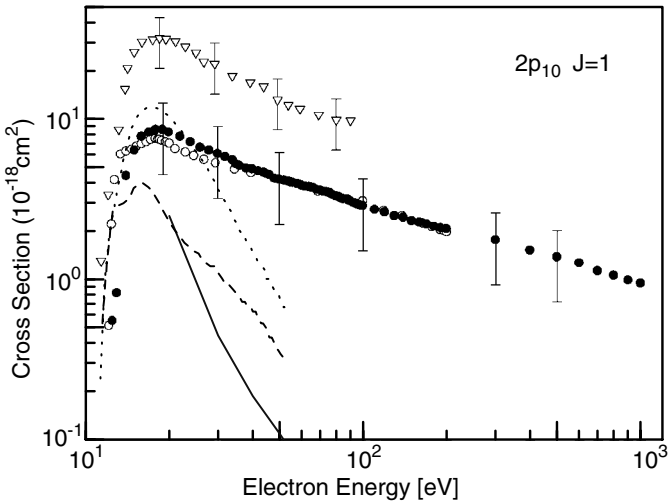

Figure 7. Cross-sections for $2p_{10}$. Apparent cross-sections: ●, present work; ○, Chilton *et al* (2000) at 2.7×10^{-1} Pa; ▽, Feltsan (1967); excitation cross-section: the dotted curve represents the distorted wave calculation DW-1 (Dasgupta *et al* 2001); long-dashed curve, 15-state BPRM result (Dasgupta *et al* 2001); full curve, distorted wave calculation MCGS (Kaur *et al* 1998).

The uncertainty in determining optical sensitivity, $k(\lambda)$, at wavelength λ depends on the wavelength range. The value estimated is 6.1% in the interval from 400 to 530 nm and 6.6% in 530 to 750 nm. Above 780 nm, the uncertainty of $k(\lambda)$ depends on the accuracy of the quoted A-coefficients of Ar (Wiese *et al* 1969, 1989). The uncertainty is the sum of estimated values for each factor. It is 25.9% for $k(\lambda)$ at 794.8 nm, 27.1% at 800.6 nm, 18.1% at 826.4 nm, 16.6% at 840.8 nm, 18.3% at 842.4 nm and 20.7% at 852.1 nm. The relative uncertainty of 2% was estimated in pressure calibration by a capacitance manometer. Intensity measurement of the standard light source was reproducible within 1.7%. It is noteworthy that the $k(\lambda)$ values thus obtained agreed within 2% with values estimated using well established He I emission cross-sections of van Zyl *et al* (1980) at 728, 505, 444 and 417 nm.

The energy dependence differs considerably from results of Feltsan (1967), especially for $2p_4 \rightarrow 1s_3$ (805.95 nm line), $2p_5 \rightarrow 1s_4$ (758.74 nm line), $2p_7 \rightarrow 1s_4$ (829.81 nm line) and $2p_{10} \rightarrow 1s_5$ (892.86 nm line) transitions, probably because of their too-high target pressure. Figure 8 shows the pressure effect on the emission cross-section for the $2p_5 \rightarrow 1s_4$ transition (758.7 nm line). The second maximum around 60 eV rose when target pressure increased to 3.5×10^{-2} Pa, while the first maximum around 20 eV did not show such behaviour, which implies that two different excitation pathways are involved. This inference is consistent with figure 2.

Bogdanova and Yurgenson (1987) used a pulsed-beam method to reduce the effect of cascade transitions to the $2p_i$ state. Their results show similar energy dependences as the present ones although the magnitude differs among several transitions. Chilton *et al* (2000) made systematic measurements on emission cross-sections for the 5p → 5s transitions as well as cascade cross-sections to the 5p levels. Their results, shown in figures 4–7, were all acquired at a target pressure of 2.7×10^{-1} Pa and are pressure dependent. Their emission cross-sections obtained at 1.3×10^{-2} Pa are also plotted at 100 eV. The result of the apparent excitation cross-section of Chilton *et al* (2000) for $2p_7$ shows a large difference from the present result, as shown in figure 6.

Table 1. 5p → 5s emission cross-sections and $Q^{apparent}$ (in 10^{-18} cm^2, at 100 eV) of Kr I. The upper line indicates the emission line wavelength (nm). Both the Paschen and Racah notations are indicated.

	Lower level				
Upper level	$1s_2$ $5s'[1/2]^o_1$	$1s_3$ $5s'[1/2]^o_0$	$1s_4$ $5s[3/2]^o_1$	$1s_5$ $5s[3/2]^o_2$	Apparent cross section $Q^{apparent}$
$2p_1$	768.52 nm		557.313		
$5p'[1/2]_0$	2.2 ± 00.49	—	0.002[a]	—	2.20
$2p_2$	826.324		587.092	556.222	
$5p'[3/2]_2$	4.3 ± 1.7	—	0.087[a]	0.013[a]	4.4
$2p_3$	828.104	785.482	587.990	557.028	
$5p'[1/2]_1$	0.34[a]	0.49 ± 0.14	0.0017[a]	0.024[a]	0.86
$2p_4$	850.887	805.950	599.385	567.245	
$5p'[3/2]_1$	0.53 ± 0.15	0.47 ± 0.14	0.0015[a]	0.0004[a]	1.00
$2p_5$	1212.347		758.741		
$5p[1/2]_0$	0.014[a]	—	3.83 ± 0.80	—	3.84
$2p_6$	1373.886		819.005	760.154	
$5p[3/2]_2$	0.036[a]	—	1.05[a]	3.20 ± 0.70	4.29
$2p_7$	1404.57	1286.189	829.810	769.453	
$5p[3/2]_1$	0.0045[a]	0.006[a]	1.70 ± 0.49	0.25[a]	1.96
$2p_8$	1547.402		877.674	810.436	
$5p[5/2]_2$	0.025[a]	—	6.85[a]	2.78 ± 0.81	9.70
$2p_9$				811.290	
$5p[5/2]_3$	—	—	—	3.20 ± 0.97[b]	3.20
$2p_{10}$	1878.545	1672.648	975.175	892.869	
$5p[1/2]_1$	0.008[a]	0.014[a]	0.35[a]	2.5 ± 1.2	2.9
Total	7.5 ± 2.4	0.98 ± 0.28	13.9 ± 3.7	12.0 ± 3.8	34.4

[a] Cross-sections were derived using transition probabilities of Dzierżęga *et al* (2000). [b] The emission cross-section for the $2p_9 \rightarrow 1s_5$ transition (811.3 nm line) of Kr reported previously was too large, because of the difficulty of determining the absolute sensitivity of the detection system above 800 nm wavelength (Tsurubuchi and Kobayashi 2002).

The theoretical calculation of level excitation cross-section by the DW-1 method included relativistic corrections in optimizing the bound-state wavefunctions (Dasgupta *et al* 2001). For the sake of clarification, the excitation cross-section of the DW-1, R-matrix (close-coupling-type) calculation with 15 states and RDW(MCGS) (Kaur *et al* 1998) are illustrated. The DW-1 result shows good agreement with the experimental result for the $2p_1$ and $2p_5$, while magnitudes of the 15-state BPRM for $2p_1$ and $2p_5$ were larger than the experimental value and were multiplied by 0.1 and 0.2 respectively. Theoretical and experimental results for the $2p_2$, $2p_3$, $2p_4$, $2p_7$, $2p_8$ and $2p_9$ states show roughly similar energy dependences below 50 eV regardless of their differences in magnitude; however, the RDW(MCGS) results for the $2p_2$ and $2p_8$ states show different behaviour. Above 50 eV, experimental apparent cross-sections all show slower energy dependences compared with theoretical ones. As mentioned before, the experimental $Q^{apparent}_{2p_i}$ includes cascade cross-sections contributing to the population of the $2p_i$ state.

The $2p_9 \rightarrow 1s_5$ transition (811.29 nm line), in the Paschen notation, is of particular interest because the $2p_9$ state is a pure triplet state and is well represented by the $^3D_3$ term in the LS scheme. Theoretical excitation cross-sections of the $2p_9$ state show almost $\sim E^{-3}$ dependence on electron energy E, whereas experimentally obtained results decrease more slowly at high energies. Feltsan (1967) and Chilton *et al* (2000) also reported this trend. For He,

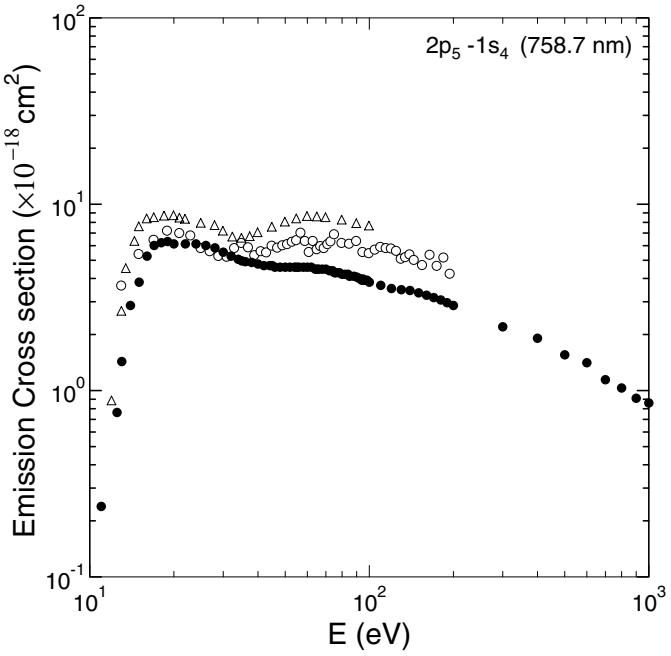

Figure 8. Target-pressure effect on the emission cross-section for the $2p_5 \rightarrow 1s_4$ transition. ●, 4.0×10^{-3} Pa; ○, 3.5×10^{-2} Pa; △, Feltsan (1967).

experimentally obtained emission cross-sections for the $3\ ^3D \rightarrow 2\ ^3P$ transition (587.6 nm line) show a slower decrease with impact energies than the result of CCC calculation including cascade transitions (Cvejanović *et al* 2000, Chilton and Lin 1998), while for the $3\ ^3P \rightarrow 2\ ^3S$ transition (388.9 nm line), agreement between experimental and theoretical results seems better (Anderson *et al* 1973, Van Raan *et al* 1974, Showalter and Kay 1975, Igual-Ruiz *et al* 2001), as shown in figure 9.

One concern, that spectral blending to the 811.29 nm line may exist because of the effect of second-order diffraction, was checked carefully using a colour filter that eliminated the Kr I 405.65 nm line ($6f[3/2]_1 \rightarrow 5s'[1/2]^o_0$) and the Kr II 405.70 nm line ($5p'\ ^2P^o_{1/2} \rightarrow 5s'\ ^2D_{3/2}$). Another possibility is that the degree of cascade cross-sections to the $2p_9$ state is remarkable at high energies, as mentioned above. One cascade emission cross-section for the $2p_9$ state, the 645.6 nm line ($6d[7/2]_4 \rightarrow 5p[5/2]_3$), was found to have a similar energy dependence as the $2p_9 \rightarrow 1s_5$ emission cross-section as given in figure 6.

A preliminary test of a time-resolving experiment was undertaken to better clarify the excitation mechanism of the $2p_9$ level (Tsurubuchi and Kobayashi 2002). An electron beam was modulated by fast rectangular pulses of 100 kHz repetitions. The decaying light emission was wavelength selected by a monochromator and monitored with a digital oscilloscope and a multi-channel analyser. Two-level analysis was tentatively applied, i.e. all cascade transitions were apparently compressed into one decaying curve with a composite decay time. It was noted that the cascade contribution to the population of the $2p_9$ state was considerable.

Although Bogdanova and Yurgenson (1987) used a pulsed beam of 15 ns duration to reduce the effect of cascade transitions, we found that the effect was considerably large and must be subtracted to have level excitation cross-sections. Further accumulation of experimental data regarding the population mechanism of the $2p_9$ level is necessary to resolve the degree to which population is caused by direct excitation and to what degree it is caused by cascade transitions.

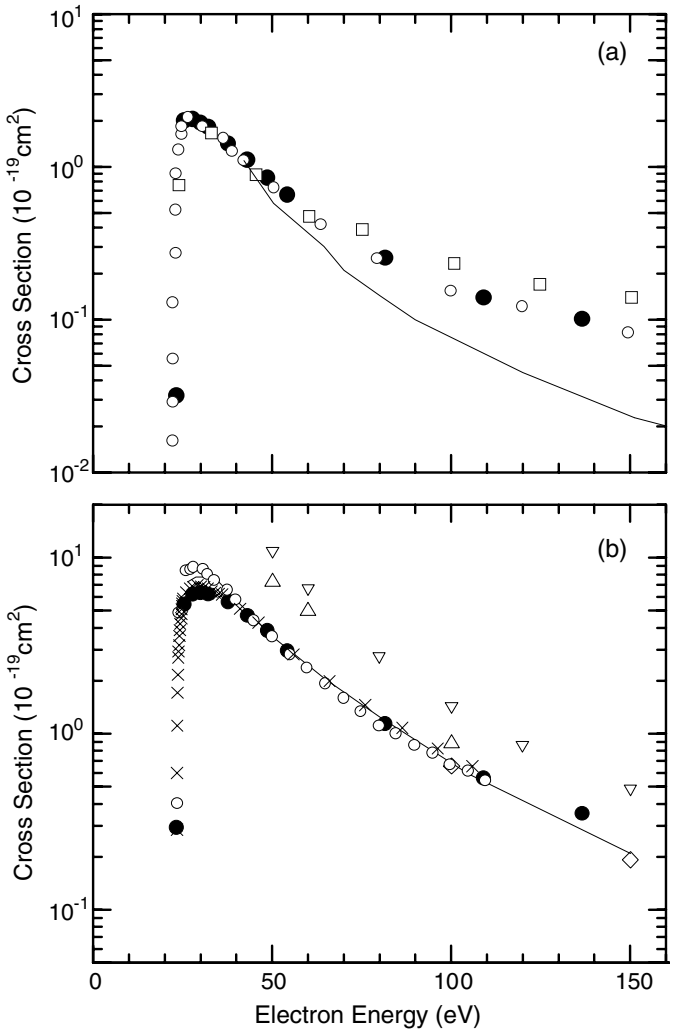

Figure 9. Emission cross-sections of He by electron impact: (a) for the $3\,^3\mathrm{D} \rightarrow 2\,^3\mathrm{P}$ (587.5 nm) line; ●, present result; □, Chilton and Lin (1998); ○, Cvejanović *et al* (2000); full curve, CCC calculation of Cvejanović *et al* (2000); (b) for the $3\,^3\mathrm{P} \rightarrow 2\,^3\mathrm{S}$ (388.9 nm) line; ●, present result; ∇, Anderson *et al* (1973); ◇, Van Raan *et al* (1974); △, Showalter and Kay (1975); ×, Gay *et al* (1996); ○, Igual-Ruiz *et al* (2001); full curve, CCC calculation of Igual-Ruiz *et al* (2001).

3.2. Emission cross-sections of the $5s \rightarrow 4p$ *resonance lines*

Because of strong self-absorption, relative emission cross-sections for the 116.49 and 123.58 nm lines at effectively zero target pressure were obtained by extrapolation of data points as a function of target pressure. Figure 10 shows experimentally obtained transmission curves. Solid curves in the figure were calculated by

$$T_R = \frac{\int_0^\infty E(\upsilon)\exp\{-K(\upsilon)l\}\,\mathrm{d}\upsilon}{\int_0^\infty E(\upsilon)\,\mathrm{d}\upsilon}, \tag{4}$$

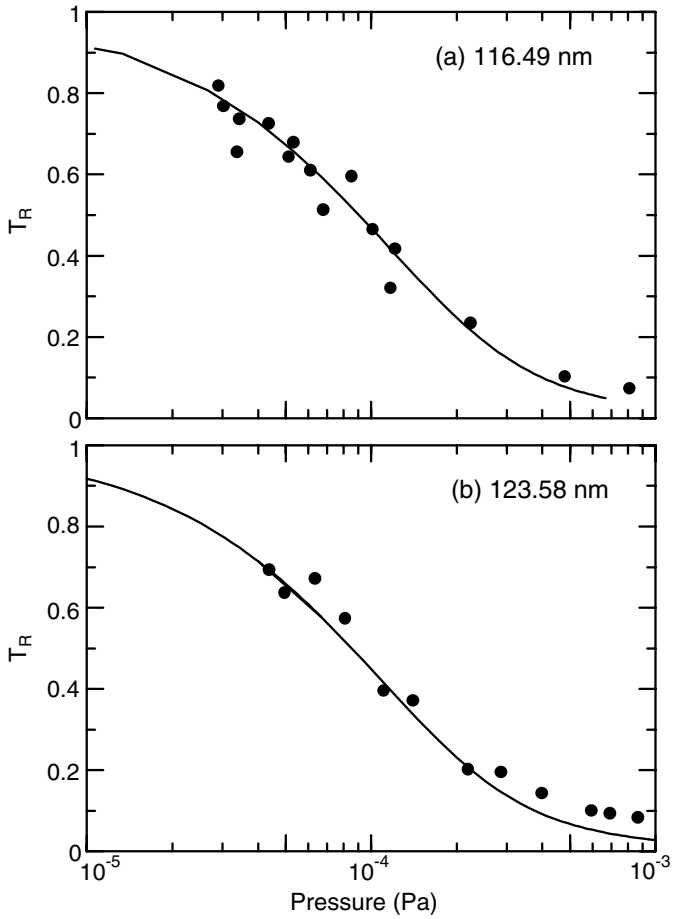

Figure 10. Transmission curve T_R of the resonance line: (a) 116.49 nm line; (b) 123.58 nm line as a function of target pressure. The optical pass length of the present setting for VUV radiation is 48.0 cm, which is the distance between the centre of the chamber and the entrance slit of the VUV monochromator.

where $E(\upsilon)$ is the frequency distribution of radiation intensity, $K(\upsilon)$ is the absorption coefficient of Kr gas and l is the optical distance. Optical oscillator strength $f(1s_2) = 0.139 \pm 0.010$ and $f(1s_4) = 0.155 \pm 0.011$ (Tsurubuchi *et al* 1989) were used in the calculation.

As mentioned previously, absolute calibration of detection efficiency in the VUV region was obtained by comparing measured intensities of the band spectra of H_2 with those calibrated ones presented by Shemansky *et al* (1985). Resultant emission cross-sections are $(21.2 \pm 5.9) \times 10^{-18}$ cm^2 for the 116.49 nm line and $(35.5 \pm 9.9) \times 10^{-18}$ cm^2 for the 123.58 nm line at 100 eV if the value of 7.3×10^{-18} cm^2 at 100 eV were used as an absolute emission cross-section for the hydrogen Ly-α line produced in electron impact of H_2.

The most prominent error is uncertainty of about 12% in the standard Lyman-α cross-section. The reproducibility of the detection efficiency curve is about 5.5% at 121.6 nm. The uncertainty in the S/IP value of resonance lines at effectively $P \to 0$ is about 5%. Lyman-α line fluctuation was within 3%. The relative excitation function was normalized to the obtained absolute value at 100 eV. Absolute measurements with much lower uncertainties have been reported for non-resonant VUV lines (Jans *et al* 1995, 1997).

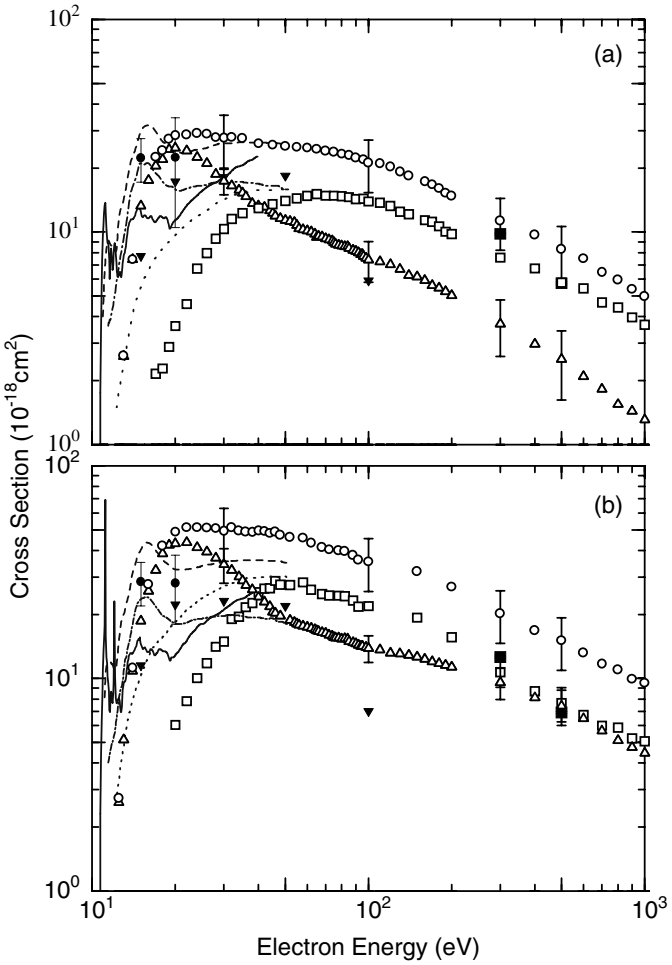

Figure 11. Open circles represent emission cross-sections for the 116.49 nm line (a) and 123.58 nm line (b); Δ, the sum of cascade cross-section; □, level excitation cross-sections for $1s_2$ (a) and for $1s_4$ (b); ■, Takayanagi *et al* (1990); ▼, Trajmar *et al* (1981). The dotted curves represent the DW-1 results; dash–dotted curves, five-state BPRM results; long-dashed curves, 15-state BPRM results; full curves, 51-state BPRM (Dasgupta *et al* 2001).

Figure 11 shows results of emission cross-sections for the resonant transitions, as well as the level excitation cross-section of the $1s_2$ and $1s_4$ states. The figure also shows the total cascade cross-section contributing to emission cross-sections. The summed cascade cross-section reaches its maximum around 20 eV and occupies most of the emission cross-section of the resonance line.

3.3. Level excitation cross-section of the $1s_2$ and $1s_4$ states

Level excitation cross-sections of the $1s_2$ and $1s_4$ states were obtained by subtracting the total cascade $5p \rightarrow 5s$ cross-sections from emission cross-sections of 116.49 and 123.58 nm resonance lines. The contribution from the 6p states was neglected. Obtained values at 100 eV are $(13.7 \pm 8.3) \times 10^{-18}$ cm^2 and $(22 \pm 14) \times 10^{-18}$ cm^2 for the $1s_2$ and $1s_4$ states, respectively, as given in table 2.

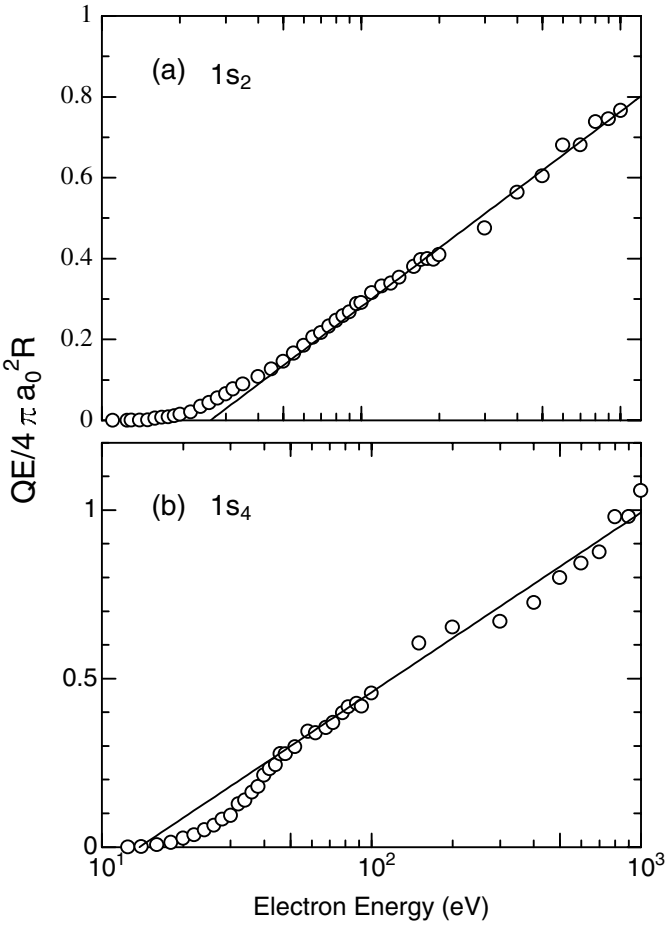

Figure 12. Fano plot for the $1s_2$ and $1s_4$ states.

Table 2. Estimation of level excitation cross-sections for the $1s_2$ and $1s_4$ levels of Kr at 100 eV in units of $10^{-18}cm^2$.

	5s levels	
	$1s_2$, $5s'[1/2]^o_1$	$1s_4$, $5s[3/2]^o_1$
Emission cross-section for the 5s → 4p resonance line	21.2 ± 5.9	35.5 ± 9.9
Sum of the 5p → 5s emission cross-sections	7.5 ± 2.4	13.9 ± 3.7
Level excitation cross-section	13.7 ± 8.3	22 ± 14

In comparing the obtained level-excitation cross-sections with those of energy-loss measurements, it was found that present results at high energies, 300 and 500 eV, agree quite well with results of Takayanagi *et al* (1990) for both $1s_2$ and $1s_4$ states. Although the value of Trajmar *et al* (1981) at 50 eV agrees with our result, the cross-section at 100 eV seems too small compared with the present result. The trend of energy dependence of the level-excitation cross-section at high energies apparently differs from the result of Takayanagi *et al* (1990).

The energy resolution in the present work was insufficient to resolve a hump in the level-excitation cross-section just after the threshold indicated by results of *R*-matrix (close-coupling-type) calculations with a varying number of states (five-, 15- and 51-state coupling), while the DW-1 result shows a monotonic increase at low energies (Dasgupta *et al* 2001).

The level excitation cross-section Q_n for level n is well expressed by the Bethe–Born approximation at high energies; it is given by

$$Q_n = \frac{4\pi a_0^2}{E/R} \frac{f_n}{E_n/R} \ln \frac{C_n E}{R}, \tag{5}$$

where a_0 is the Bohr radius, R is the Rydberg constant, E_n represents the excitation energy of the nth level, C_n is a constant and f_n is the optical oscillator strength of the state. The Fano plot above 100 eV gives $f_n(1s_2) = 0.164 \pm 0.011$, $C_n = 0.52$, and $f_n(1s_4) = 0.171 \pm 0.030$, $C_n = 0.99$, for the $1s_2$ and $1s_4$ states, respectively, by the method of least-squares minimum, as shown in figure 12. These values can be compared with $f(1s_2) = 0.1496 \pm 0.0038$ and $f(1s_4) = 0.1751 \pm 0.0049$ presented by an absolute self-absorption technique (Ligtenberg *et al* 1994). That fact indicates that the obtained energy dependence of the level excitation function is satisfactory.

4. Summary

A set of electron-impact emission cross-sections of Kr I was measured in a wide range of impact energies from the threshold to 1000 eV for the $5p \rightarrow 5s$ transition in the visible to near infrared regions at sufficiently low target pressure. A main reason for scattering among experimental data is the too-high target pressure used in previous studies. In general, the energy dependence of the emission cross-section at high energies was found to descend more slowly than the result of theoretical calculations, probably because of the large cascade effect to the 5p states, which must be resolved by further experimental and theoretical study.

We obtained absolute emission cross-sections for the $5s \rightarrow 4p$ resonance lines (116.49 and 123.58 nm) by normalizing relative emission cross-sections at effectively zero target pressure to that of hydrogen Lyman-α produced in electron impact of H_2. Level excitation cross-sections of the $5s'[1/2]_1^o$ and $5s[3/2]_1^o$ states ($1s_2$ and $1s_4$ respectively in the Paschen notation) were obtained and compared with results of energy-loss measurements and calculated cross-sections using distorted wave and close-coupling approaches. The obtained energy dependence of excitation cross-section at high energies was found fairly well through careful examination of optical oscillator strengths given in the Fano plot.

Acknowledgment

This work was partly supported by a Grant-in-Aid for Scientific Research (B) from the Japan Society for Promotion of Science. It was carried out under the 21st Century COE (Centre of Excellence) programme 'Future nano-materials' in Tokyo University of Agriculture and Technology.

References

Ajello J M, Shemansky D E, Franklin B, Watkins J, Srivastava S, James G K, Simms W T, Hord C W, Pryor W, McClintock W, Argabright V and Hall D 1988 *Appl. Opt.* **27** 890–914

Anderson R J, Hughes R H, Tung J H and Chen S T 1973 *Phys. Rev.* A **8** 810–15

Bogdanova I P and Yurgenson S V 1987 *Opt. Spectrosc.* **62** 424–5

Chilton J E and Lin C C 1998 *Phys. Rev.* A **58** 4572–80
Chilton J E, Stewart M D Jr and Lin C C 2000 *Phys. Rev.* A **62** 032714
Cvejanović D, Clague K, Fursa K, Bartschat K, Bray I and Crowe A 2000 *J. Phys. B: At. Mol. Opt. Phys.* **33** 2265–78
Dasgupta A, Bartschat K, Vaid D, Gurm-Grzhimalio A N, Madison D H, Blaha M and Giuliani J L 2001 *Phys. Rev.* A **64** 052710
Dzierżęga K, Volz U, Nave G and Griesmann U 2000 *Phys. Rev.* A **62** 022505
Feltsan P V 1967 *Ukr. Fiz. Zh.* **12** 1424–9
Gay T J, Furst J E, Trantham K W and Wijayaratna W M K P 1996 *Phys. Rev.* A **53** 1623–9
Guo X, Mathews D F, Mikaelian G, Khakoo M A, Crowe A, Kanik I, Trajmar S, Zeman V, Bartschat K and Fontes C J 2000 *J. Phys. B: At. Mol. Opt. Phys.* **33** 1895–919
Igual-Ruiz N, Donnelly B P, McLaughlin D T, Cvejanovic D, Crowe A, Fursa D, Bartschat K and Bray I 2001 *J. Phys. B: At. Mol. Opt. Phys.* **34** 2289–300
Jans W, Möbus B, Kühne M and Ulm G 1997 *Phys. Rev.* A **55** 1890–8
Jans W, Möbus B, Kühne M, Ulm G, Werner A and Schartner K H 1995 *Appl. Opt.* **34** 3671–80
Kaur S, Srivastava R, McEachran R P and Stauffer A D 1998 *J. Phys. B: At. Mol. Opt. Phys.* **31** 4833–52
Ligtenberg R C G, McPherson A, Rouze N, Westerveld W B and Risley J S 1985 *Proc. 14th Int. Conf. on Physics of Electronic and Atomic Collisions (Palo Alto)* p 276 (Abstracts)
Ligtenberg R C G, van der Burgt, Renwick S P, Westerveld W B and Risley J S 1994 *Phys. Rev.* A **49** 2363–80
Massey H S W and Burhop E H S 1969 *Electronic and Ionic Impact Phenomena* vol 1 (Oxford: Clarendon) p 170
Shemansky D E, Ajello J M and Hall D T 1985 *Astrophys. J.* **296** 765–73
Showalter J G and Kay R B 1975 *Phys. Rev.* A **11** 1899–910
Takayanagi T, Li G P, Wakiya K, Suzuki H, Ajiro T, Inaba T, Kano S and Takuma H 1990 *Phys. Rev.* A **41** 5948–52
Trajmar S, Srivastava S K, Tanaka H, Nishimura H and Cartwright D C 1981 *Phys. Rev.* A **23** 2167–77
Tsurubuchi S 1997 *J. Phys. Soc. Japan* **66** 3070–73
Tsurubuchi S, Arakawa K, Kinokuni S and Motohashi K 2000 *J. Phys. B: At. Mol. Opt. Phys.* **33** 3713–23
Tsurubuchi S and Kobayashi H 2002 *Correlations, Polarization, and Ionization in Atomic Systems (AIP Conf. Proc. No 604)* ed D H Madison and M Schulz (New York: American Institute of Physics) pp 166–71
Tsurubuchi S, Miyazaki T and Motohashi K 1994 *J. Phys. Soc. Japan* **63** 3996–9
Tsurubuchi S, Miyazaki T and Motohashi K 1996 *J. Phys. B: At. Mol. Opt. Phys.* **29** 1785–801
Tsurubuchi S, Motohashi K, Matsuoka S and Arikawa T 1991 *Chem. Phys.* **155** 401–6
Tsurubuchi S, Watanabe K and Arikawa T 1989 *J. Phys. B: At. Mol. Opt. Phys.* **22** 2969–75
Van Raan A F J, Moll P G and van Eck J 1974 *J. Phys. B: At. Mol. Phys.* **7** 950–65
van Zyl B, Dunn G H, Chamberlain G and Heddle D W O 1980 *Phys. Rev.* A **22** 1916–29
van Zyl B, Gealy M W and Neumann H 1985 *Phys. Rev.* A **31** 2922–31
Wiese W L, Brault J M, Danzmann K, Helbig V and Kock M 1989 *Phys. Rev.* A **39** 2461–71
Wiese W L, Bridges J M, Kornblith R L and Kelleher D E 1969 *J. Opt. Soc. Am.* **59** 1206–12
Woolsey J M, Forand J L and McConkey J W 1986 *J. Phys. B: At. Mol. Phys.* **19** L493–7